Journal of Solid State Electrochemistry
https://doi.org/10.1007/s10008-020-04727-7

ORIGINAL PAPER

# Efficiency enhancement in dye-sensitized solar cells using hierarchical $TiO_2$ submicron size spheres as a light scattering layer

M. A. K. L. Dissanayake [1] · S. Senthuran [1,2,3] · G. K. R. Senadeera [1,4]

Received: 22 March 2020 / Revised: 13 June 2020 / Accepted: 15 June 2020


## Abstract

The photoanode of a dye-sensitized solar cell (DSSC), usually made with a nanoporous $TiO_2$ semiconductor layer sensitized with N719 dye, plays a crucial role in the overall power conversion efficiency as it influences both the light absorption and the electron transport. Generally, enhanced photon absorbance is achieved through light scattering in the device by employing a double-layered $TiO_2$ photoanode consisting of an active layer of smaller (~ 20 nm) P25 particles and a scattering layer consisting of larger (~ 300 nm) particles. However, due to the smaller effective surface area of the larger particle layer, the dye adsorption in the second layer is very poor, and therefore, the efficiency enhancement due to the usage of thicker photo anode is hindered. Therefore, in this study, investigations were carried out to replace the conventional, larger particle scattering layer by a morphologically different structure of $TiO_2$. Here, the DSSC performance between two different types of scattering layers, one consisting of $TiO_2$ nanorods (NRs) and the other consisting of hierarchically structured $TiO_2$ submicron size spheres (MS) are compared. DSSC fabricated with P25/MS double-layered photoanode outperforms the DSSC fabricated with P25/NR double-layered photoanode. P25/MS-based DSSC delivered a highest short-circuit current density of 14.80 mA $cm^{-2}$ with an efficiency of 7.38%, while the efficiency of DSSC fabricated with P25/NR photoanode exhibits 7.03% efficiency. The DSSC fabricated without a scattering layer showed only 6.68% efficiency. The diffuse reflectance and dye adsorption measurements revealed that the better performance of P25/MS double-layered DSSC is largely due to the improved photon absorption facilitated by superior light scattering as well as higher dye loading by $TiO_2$ submicron size spheres.

**Keywords** Dye-sensitized solar cells · Photoanode · Light scattering · Hierarchical $TiO_2$ submicron size spheres

## Introduction

Investigations on dye-sensitized solar cells (DSSCs) have been intensively carried out in the last three decades due to their promising features such as low production cost with easy fabrication techniques, relatively high power conversion efficiency especially under diffused light conditions, environmentally friendly fabrication process in ambient conditions, and tunable esthetic features, such as color and transparency [1–6]. Typically, a DSSC consists of a photoanode of high band gap semiconductor like $TiO_2$, a dye sensitizer, an electrolyte with redox mediator and a counter electrode assembled in a sandwiched structure. When this structure is exposed to the light, dye molecules adsorbed to the semiconducting layer get excited due to the photon energy in the light and inject electrons to the conduction band of the semiconductor producing dye cations. These electrons then traverse to the other side of the device via the external circuit and transferred to the redox mediator in the electrolyte through the counter

**Highlights** • Dye-sensitized solar cells with $TiO_2$ submicron size sphere photoanode were studied.
• Cells with $TiO_2$ P25 particle/nanorod double layer showed efficiency of 7.03%.
• Cells with $TiO_2$ P25 particle/submicron sphere anode showed efficiency of 7.38%.
• Higher efficiency was attributed to enhanced light absorption by scattering.

✉ M. A. K. L. Dissanayake
lakshman.di@nifs.ac.lk

[1] National Institute of Fundamental Studies, Kandy, Sri Lanka
[2] Department of Physics, University of Jaffna, Jaffna, Sri Lanka
[3] Postgraduate Institute of Science, University of Peradeniya, Peradeniya 20400, Sri Lanka
[4] Department of Physics, The Open University of Sri Lanka, Nugegoda, Sri Lanka

Published online: 23 June 2020

electrode. Due to the redox reaction of the mediator in the electrolyte, electrons are released and the dye cations return to their ground state molecules receiving these electrons. To date, the highest power conversion efficiency of ~ 14.3% under one sun illumination has been reported for a DSSC using $TiO_2$ as a semiconductor metal oxide photoanode and alkoxysilyl-anchor dye (ADEKA-1) and carboxy-anchor organic dye (LEG4) as a co-photosensitizer, cobalt(III/II) complex as a redox electrolyte, and graphene-based gold-coated fluorine-doped tin oxide as the counter electrode [5].

Due to aforementioned promising properties of DSSCs, continued research efforts are being focused towards improving the performance of DSSCs by optimizing photoanode [7–11], sensitizer [12–15], electrolyte [16–18], and counter electrode [19–22]. Among these components, the architecture of photoanode plays a crucial role in the overall power conversion efficiency of the solar cell because the dye adsorption, electron generation, and transport take place in the photoanode. Thus, optimizing the architecture of photoanode to boost the solar cell performance is strategically an important step.

A photoanode with high specific surface area, fast electron transport pathways, and pronounced light scattering schemes are desirable for achieving higher efficiencies. Usually, the photoanode is made of ~ 20 nm diameter $TiO_2$ nanoparticles as a nanoporous structure. This structure provides a large internal surface area for the adsorption of large amount of dye molecules on the surface of the $TiO_2$ layer in order to absorb as much as incident light as possible. Therefore, the efficiency of these devices can be enhanced by increasing the thickness of this nanoparticle layer. However, due to the diffusion length of electron and low light penetration, there is a limit of increasing the thickness of the photoanode. Therefore, enhancement in the light absorption by the dye molecules by means of an efficient light scattering process thorough the photoanode is one of the possible strategies to enhance the efficiency of these solar cells. Conventionally, this is achieved by using a double-layered $TiO_2$ photoanode structure. For this purpose, a light scattering layer consisting of larger particles of sizes ~ 300 to 700 nm in diameter is fabricated on top of the smaller size (~ 20 nm diameter) $TiO_2$ nanoparticle layer [23]. However, the top layer only serves as a scattering layer, and it does not contribute significantly for dye adsorption and light absorption because of its low specific surface area. Therefore, in order to enhance the efficiency of these devices, it is better to employ a photoanode structure with high dye adsorption capability together with enhanced light scattering within the device.

Recently, much research interests have been focused towards the utilization of $TiO_2$ nanomaterials such as nanowires [24], nanorods [25], nanofibers [26], nanospindles [27], and hierarchically structured submicron size spheres [28–30] in the photoanode and exploit their unique optoelectric properties to meet the above competing phenomena. To the best of our knowledge, there is no study carried out to compare the performance of DSSCs employing one-dimensional scattering layers such as nanorods and three-dimensional scattering layer such as hierarchically structured $TiO_2$ submicron size spheres. By having this idea in mind, in the present work, morphologically different, hierarchically structured $TiO_2$ submicron size spheres and $TiO_2$ nanorods have been successfully synthesized by hydrothermal methods. DSSCs have been fabricated with double layered photoanode structures comprising a scattering layer composed of above different morphologies and their performance have been compared.

## Materials and methods

### Materials

Fluorine-doped tin oxide (FTO)-coated conducting glasses (8 Ω $cm^{-2}$, Solaronix), titanium(IV) isopropoxide (97% Fluka), titanium dioxide powders (P-25, Degussa, and P-90, Evonik), polyethylene glycol (PEG, 99.8%, Mw = 1000 g $mol^{-1}$, Sigma-Aldrich), Triton X-100 (Sigma-Aldrich), ethanol absolute (anhydrous, > 99.8%, VWR Chemicals), glacial acetic acid (99%, Fisher), sodium hydroxide (> 98%, anhydrous, Sigma-Aldrich), ethylene carbonate (EC, Fluka), tetrapropyl ammonium iodide ($Pr_4NI$,Sigma-Aldrich), iodine chips ($I_2$, Fluka), and ruthenium dye (N719, Solaronix) were used as received.

### Synthesis

#### $TiO_2$ submicron size spheres

Hierarchically structured mesoporous $TiO_2$ submicron size spheres were synthesized through controlled hydrothermal treatment of titanium(IV) isopropoxide (TTIP) in ethanol-glacial acetic acid mixture. Typically, 1 ml TTIP was added dropwise into a mixed solvent of acetic acid (10 ml) and ethanol (50 ml) under vigorous stirring for 1 h at room temperature. The clear solution obtained was transferred into a 100-ml Teflon-lined stainless steel autoclave, and hydrothermal treatment was performed at 180 °C for 9 h. Then, the autoclave was allowed to cool down to room temperature and the resulting white precipitate was collected by centrifuge and subsequently washed with ethanol and distilled water several times and subsequently dried overnight at 90 °C. Finally, the powder sample was calcined at 400 °C for 3 h in a furnace to obtain the $TiO_2$ submicron size spheres.

#### $TiO_2$ nanorods

$TiO_2$ nanorods were synthesized via hydrothermal method. The starting material was commercial P-25 $TiO_2$ nanoparticles. In a

typical synthesis process, 0.5 g of P-25 $TiO_2$ nanoparticles were well dispersed in 70 ml of 10 M sodium hydroxide aqueous solution using a magnetic stirrer for about 1 h and subsequently sonicated in an ultrasonic bath for another 1 h. The mixture was then transferred into a 100-ml Teflon-lined stainless steel autoclave, and the hydrothermal treatment was performed at 150 °C for 48 h. Then, the autoclave was allowed to cool down to room temperature and the product was washed several times with 0.1 M HCl until a pH of 7 was reached. Finally, the $TiO_2$ nanorods were collected by centrifuging at 2000 rpm and dried at 80 °C for 12 h in a vacuum oven.

### Preparation of $TiO_2$ bi-layer photoanode

At first a compact blocking layer was spin coated (3000 rpm) on pre-cleaned FTO glass plate using a dispersion prepared with P90 $TiO_2$ powder and 0.1 M $HNO_3$. Then, the FTO plate with the blocking layer was annealed at 450 °C for 45 min. A P25 $TiO_2$ nanoparticle paste was prepared by the following method: 0.25 g of commercial P25 $TiO_2$ powder was ground with one drop of Triton X-100, 0.05 g PEG (Mw = 1000 g $mol^{-1}$), and 1 ml 0.1 M $HNO_3$ for 45 min. The P25 nanoparticle layer was formed on top of the P90 compact layer by doctor blade method, and the resulting FTO/P90/P25 photoanode was sintered at 450 °C for 45 min. The thickness of this P25 layer has already been optimized by us in a previous study [31]. A similar procedure was followed to prepare another paste by using the $TiO_2$ submicron size spheres (MS) prepared by the method described in the "TiO2 submicron size spheres" section in place of P-25 nanoparticles and applied on top of the P25 layer and sintered at 450 °C for 45 min to obtain the FTO/P90/P25/MS double-layered $TiO_2$ photoanode. The same procedure was repeated to prepare the FTO/P90/P25/NR double-layered $TiO_2$ photoanode where the top layer was $TiO_2$ nanorods prepared as described in the "TiO2 nanorods" section. Finally, these two double-layered photoanodes as well as the P25 photoanode without a scattering layer were dipped independently in ethanoic dye solution containing 0.3 mM of N719 dye at room temperature for 24 h. The average thickness of the P25 layer is about 13 μm, and the average thickness of the scattering layers is 4 μm.

### Preparation of the Pt counter electrode

Platinum counter electrodes were prepared by an electroplating experiment carried out using a two electrodes system. All solutions were prepared with deionized water, hydrogen hexachloroplatinate (IV) hydrate (Aldrich, 99.9%), and hydrochloric acid (Sigma-Aldrich, sp. gr. 1.18). The experiments were done at room temperature. Precleaned conducting glass plates were immersed in a solution of 5 mM $H_2PtCl_6$ + 0.1 M HCl, and a DC voltage 2.0 V was applied for about 2 min until shining nontransparent Pt film was deposited on the conducting glass plate. The resulting Pt film with substrate was finally heated at 200 °C for 30 min.

### Preparation of the liquid electrolyte and fabrication of solar cells

The iodide/triiodide-based liquid electrolyte used for this work was prepared by dissolving 0.738 g tetrapropylammonium iodide ($Pr_4NI$), 0.06 g iodine ($I_2$), and 3.6 ml of molten ethylene carbonate (EC) in 1 ml acetonitrile. The final mixture was magnetically stirred for 24 h at room temperature. Solar cells of configurations, double-layer photoanode with P25/MS/electrolyte/Pt counter electrode, and double-layer photoanode with P25/NR/electrolyte/Pt counter electrode, were fabricated by sandwiching the liquid electrolyte between each photoanode and the Pt counter electrode. A schematic diagram of the two solar cells is shown in Fig. 1.

### Characterization

The surface morphology of the photoanodes and synthesized nanostructures were characterized by scanning electron microscopy (SEM) using Zeiss EVO LS15 scanning electron microscope and by transmission electron microscopy (TEM) using JEOL JEM 2100 transmission electron microscope, respectively. The wide-angle X-ray spectroscopy (WAXS) was performed using Rigaku X-ray diffractometer with CuK$\alpha$ radiation ($\lambda$ = 1.5406 Å). The diffuse reflection spectra were obtained in the wavelength range from 240 to 800 nm using UV-Vis spectrophotometer (Shimadzu 2450) with an integrating sphere attachment. The amount of dye loading of the $TiO_2$ films was estimated by desorbing the dye in 0.1 M NaOH aqueous solution, and then the absorbance of the dye desorbed NaOH solution was measured using UV-vis spectroscopy. The current density–voltage (*J-V*) measurements of solar cells were performed with Keithly 2400 source meter (Keithly Instruments, USA) with solar simulator (Oriel) under 100 mW $cm^{-2}$(one sun) illumination with AM 1.5 spectral filter. The solar simulator was calibrated with a silicon photodiode (Hamamatsu Photonics, Japan). The active area of solar cells was kept constant as 0.25 $cm^2$. The interfacial charge transfer resistances and electron life time was estimated by electrochemical impedance spectroscopy (EIS) performed under 100 mW $cm^{-2}$ illumination using a Metrohm Autolab PGSTAT128N in potentiostat mode with a FRA 32 M frequency response analyzer covering the wide frequency range (0.01 Hz to 1 MHz).

## Results and discussion

Figure 2 shows the scanning electron microcopy (SEM) images of the top views of the three photoanodes fabricated with

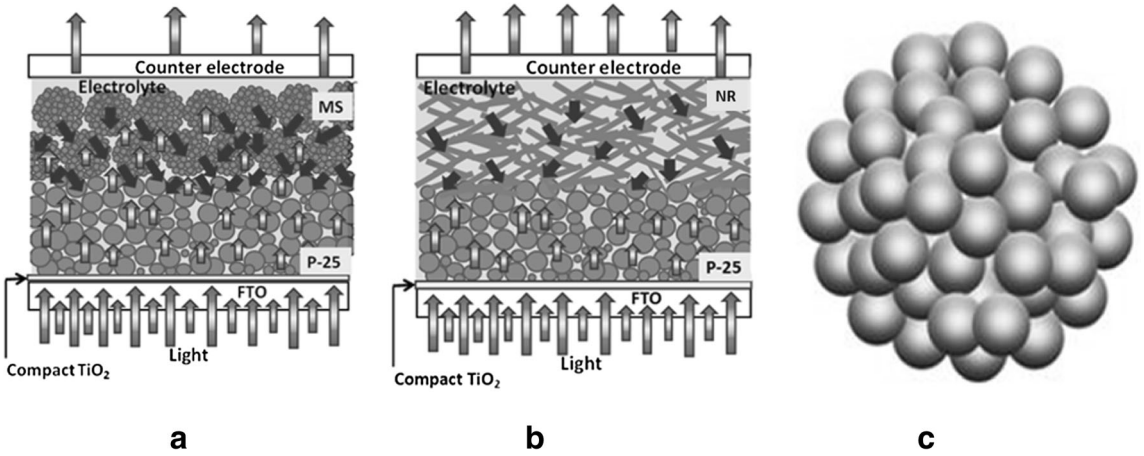


**Fig. 1** Schematic diagram of the DSSCs fabricated using **a** P25/MS-based photoanode, **b** P25/NR-based photoanode, and **c** single submicron size sphere composed of aggregates of smaller $TiO_2$ nanoparticles

P25, NR, and MS, respectively. As shown in Fig. 2a, the photoanode made only with P25 nanoparticles has a fairly uniform distribution of $TiO_2$ nanoparticles of average size around 20 nm as expected. The SEM image of randomly distributed $TiO_2$ nanorods can be seen in Fig. 2b. The SEM photograph of photoanode depicted in Fig. 2c shows that the $TiO_2$ submicron size spheres are well-defined spherical submicron size structures composed of aggregates of smaller $TiO_2$ nanoparticles. The average diameter of the submicron size spheres is about 700 nm. The diameter of the submicron size spheres can be controlled by controlling the volume ratio of the solvents used in the solution while keeping other hydrothermal conditions constant. A closer inspection of the high-resolution SEM image of the submicron size spheres (Fig. 2d) reveal that the size of the constituent much smaller nanoparticles ranges between 5 and 15 nm.

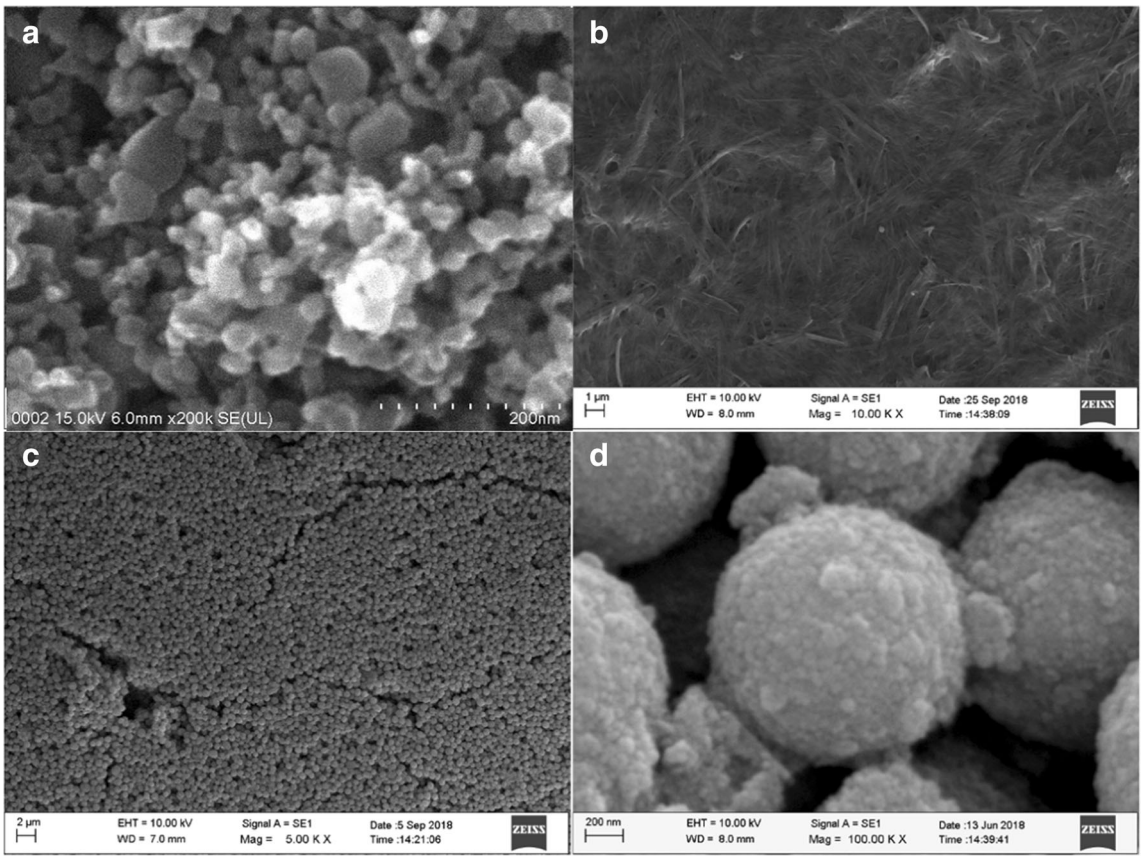


**Fig. 2** SEM images of **a** top view of $TiO_2$ P25, **b** $TiO_2$ nanorods, **c** $TiO_2$ submicron size sphere photoanodes, and **d** high-resolution image of submicron size spheres

In order to confirm the nanorod morphology, transmission electron microscope (TEM) and image was taken. Figure 3 shows the TEM of the $TiO_2$ nanorods.

Figure 3 a shows the high-resolution TEM image of a $TiO_2$ short nanorod (circled) of length about 20 nm and diameter about 5 nm. Figure 3 b shows the SEM image (an enlarged image of Fig. 2b) of randomly distributed long $TiO_2$ nanorods. The length of nanorods found in the SEM image appears to be 4–6 μm only.

Figure 4 a shows the X-ray diffraction pattern of $TiO_2$ submicron size spheres after sintering at 400 °C for 3 h in air. Diffraction peaks present at $2\theta = 25.3°$, 37.8°, 48°, 53.9°, 55.1°, 62.7°, 68.6°, and 70.3° were clearly observed and indexed by matching with reference database (JCPDS No. 21-1272) which confirms the presence of anatase phase in $TiO_2$ submicron size spheres. Figure 4 b shows the XRD of $TiO_2$ nanorods. It shows that all the prominent peaks are associated with anatase phase, and there is one less intense rutile peak also observed in the studied range.

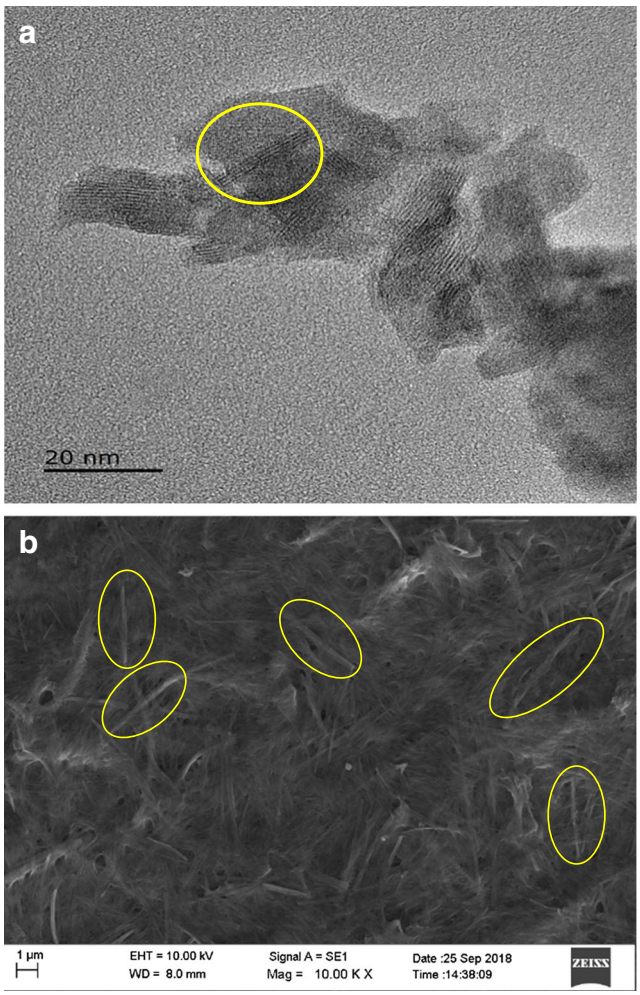


**Fig. 3** **a** TEM image of a $TiO_2$ long nanorod (circled) of length about 20 nm and diameter about 5 nm. **b** Enlarged SEM image of randomly distributed long $TiO_2$ nanorods. This image shows that the length of the nanorods is 4–6 μm

To investigate how much light is scatter back into the bottom P25 layer of double-layer structure by top MS and NR scattering layers, the diffuse reflectance of these three top layers having identical thicknesses were measured using an integrating sphere technique and results are shown in Fig. 5. According to Fig. 5, the scattering layer made of $TiO_2$ submicron size spheres exhibits the highest diffuse reflectance or in other words the highest scattering efficiency, followed by $TiO_2$ nanorod scattering layer and the $TiO_2$ nanoparticle layer in the entire wavelength range from 400 to 800 nm.

As can be seen from Fig. 5, the light scattering efficiency of $TiO_2$ nanoparticle (NP) layer shows a rapid decrease in the wavelength range from 400 to 800 nm showing its inability to scatter the light in the above wavelength range. Similar results have also been reported by the others [30, 32]. According to Mie light scattering theory, the light scattering efficiency of a thin film depends on the size of the constituent scattering particles. The submicron size spheres are more favorable for Mie scattering rather than the nanorods which have diameter in the order of nanometers. The increase in light scattering ability of the scattering layer with micron size spheres increases the optical path length within the photoanode through multiple light scattering. Therefore, both scattering layers, MS and NR, provide the "light trapping effect" within the DSSC thereby increasing the probability of rapid and efficient light absorption by the dye molecules.

As it is well known, the amount of dye adsorbed on the semiconductor layer significantly affects the power conversion efficiency of a DSSC and it is directly proportional to the short circuit current density. The estimated amounts of dye loading in above three types of photoanodes are shown in the Table 1. The highest dye adsorption of $1.21\times10^{-7}$ mol $cm^{-2}$ was achieved in microsphere based double layered P25/MS photoanode. It is well known that N719 dye adsorbs on the $TiO_2$ surface and forming a monolayer. So, it is very obvious that higher dye loading is good evidence for higher specific surface area of the hierarchically structured microsphere. The lowest dye loading was observed in P25/NR photoanode due to its one-dimensional nature. As stated in the introduction, the conventional scattering layer used in DSSCs consists of larger size $TiO_2$ single particles deposited on a $TiO_2$ P25 layer. They only increase the light scattering and do not contribute significantly for dye adsorption because of its low specific surface area. However, the hierarchically structured submicron spheres used in this work are spherical aggregates of many tiny nanoparticles and they possess a high specific surface area as evidenced by the higher dye loading. The lower dye loading in P25/NR photoanode is clearly due to low porosity of the NR scattering layer as shown in the SEM image.

Figure 6 shows the current density–voltage characteristics of DSSCs fabricated with P25/MS, P25/NR, and P25

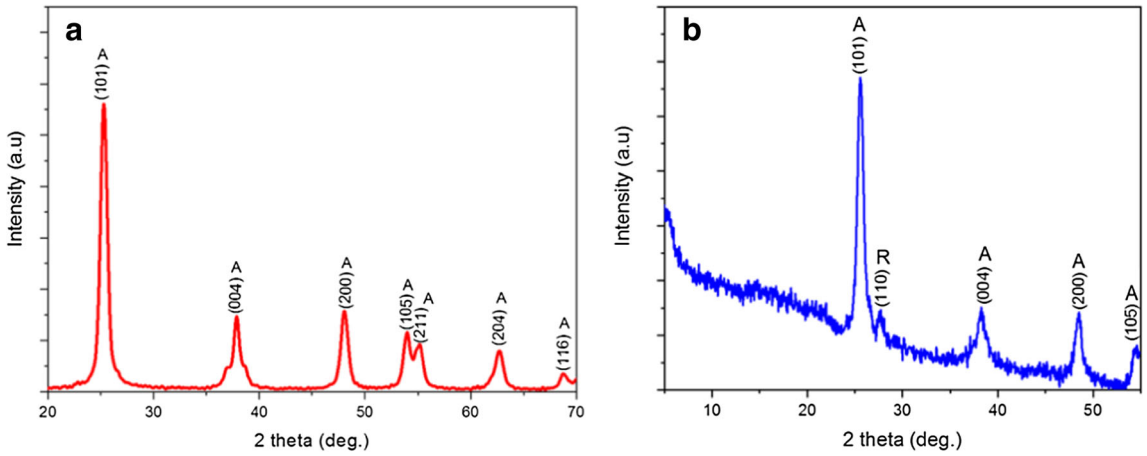


**Fig. 4** XRD pattern of **a** $TiO_2$ submicron size spheres and **b** $TiO_2$ nanorods

photoanodes under 100 mW $cm^{-2}$ illumination. The detailed solar cell parameters are summarized in Table 2. The solar cell parameters reported in the table are the average values obtained from 10 cells for each type of photoanode. DSSC fabricated with double-layered P25/MS photoanode produces the highest current density of 14.80 mA $cm^{-2}$. This could be attributed to the superior light scattering ability due to the hierarchical mesosphere structure as well as higher dye loading by $TiO_2$ submicron size spheres owning to the availability of much larger specific surface area. These arguments are well correlated with the diffuse reflectance data and dye loading measurements. The current density of the DSSC fabricated with P25/NR photoanode showed a lower value compared to the DSSC comprising with P25/MS photoanode. This is evidently due to the lower light scattering ability and lower dye loading capacity of NR scattering layer compared to the MS layer as observed previously. Even though the dye loading of P25/NR-based photoanode is lesser than the conventional P25 photoanode, the DSSCs fabricated with P25/NR photoanode shows superior short-circuit current density. This could be essentially due to the enhanced light scattering effect by the P25/NR photoanode structure. As it can be seen from both Fig. 5 and the Table 2, the lowest current density of 13.21 mA $cm^{-2}$ was observed in DSSC fabricated with P25 layer without any scattering layers. The open circuit voltage of the cells remained essentially the same with MS and NR scattering layers but the values are lower than for the P25 cell. The fill factors of double-layered solar cells were slightly higher than the DSSCs with single-layered P25 cell. This could be due to better infiltration of liquid electrolyte through the porous network of scattering layers [33]. Therefore, it is evident from the table that a significantly higher efficiency ($\eta$) can be achieved by employing a $TiO_2$ MS layer on the conventional $TiO_2$ P25 photoanode.

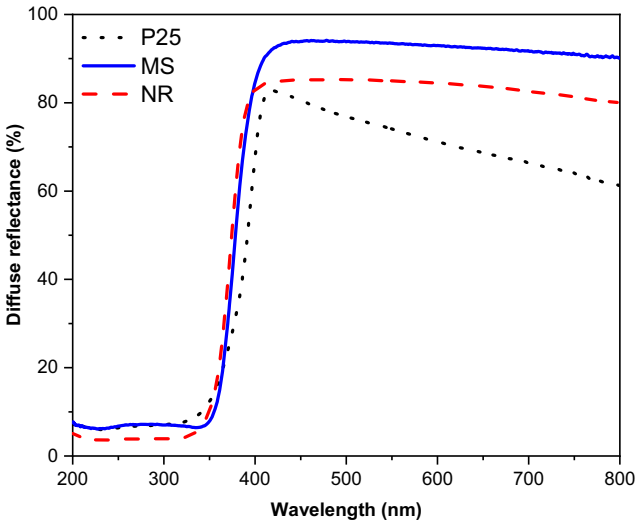


**Fig. 5** Diffuse reflectance spectra of MS and NR scattering layers compared with P25 layer

The electrochemical impedance spectroscopy (EIS) measurements have been widely employed as an important diagnostic tool in electrochemistry to estimate the interfacial resistances and also to understand the charge transfer mechanism at the interfaces of electrochemical systems including DSSCs. There are four interfaces in a DSSC, namely, FTO/$TiO_2$, $TiO_2$/dye, dye/electrolyte, and electrolyte/counter electrode. A typical Nyquist plot of a DSSC has three semicircles in high-frequency, intermediate-frequency, and low-frequency regions, respectively. Figure 7 shows the (a) Nyquist plots and corresponding Bode plots (b) obtained from EIS measurements for DSSCs fabricated with different photoanode structures under the same illuminating conditions (1000 W $m^{-2}$).

**Table 1** The amount of dye loading on P25, P25/NR, and P25/MS photoanodes

| Photoanode | Adsorbed dye ($\times 10^{-7}$ mol $cm^{-2}$) |
|---|---|
| P25 | 1.09 |
| P25/NR | 0.96 |
| P25/MS | 1.21 |

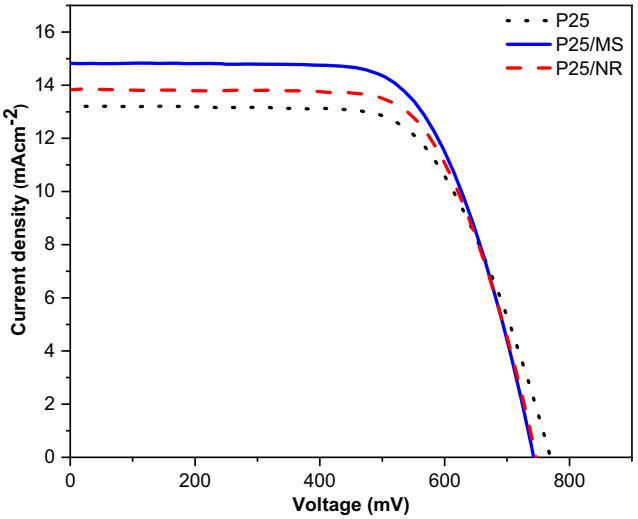


**Fig. 6** Current density–voltage (*J-V*) curves of DSSCs fabricated with double layer (P25/MS and P25/NR) and single layer (P25) $TiO_2$ photoanodes

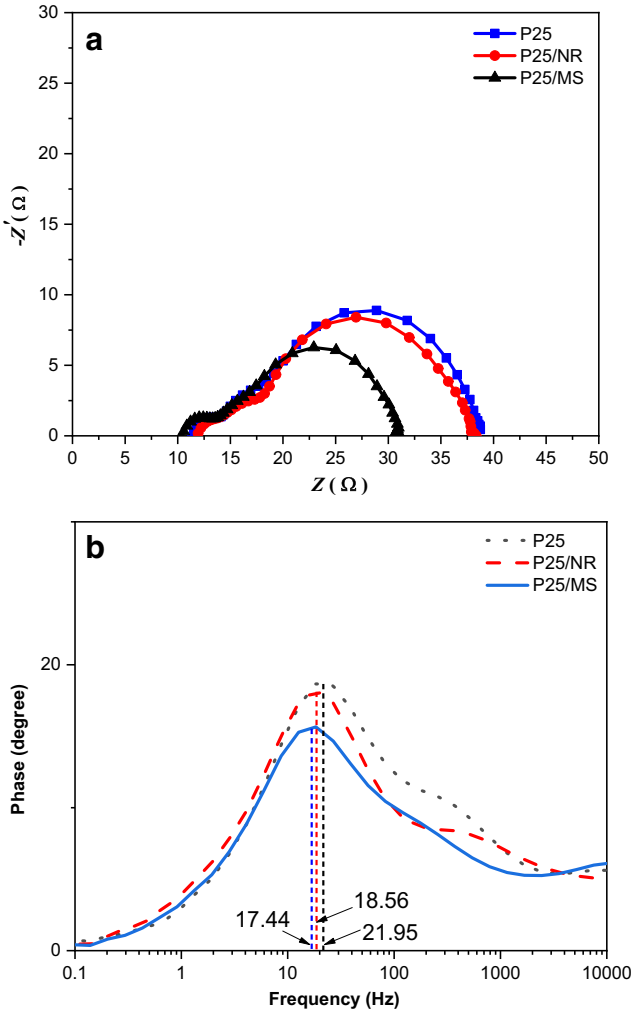


**Fig. 7** **a** Nyquist plot and **b** Bode plot of double-layer and single-layer DSSC measured under 100 mW $cm^{-2}$ illumination

As depicted in Fig. 7a, two semicircles can be seen in the Nyquist plots of these devices. The charge transfer resistance values were extracted by fitting the impedance data with an appropriate equivalent circuit model as shown in the inset of Fig. 7a by using NOVA software. The smaller semicircle in the higher frequency region attributed to the charge transfer resistance ($R_1$) of the electrolyte/counter electrode interface. The larger semicircle in the intermediate-frequency region ascribed to the charge transfer resistance ($R_2$) of the dye-loaded $TiO_2$ electrode/electrolyte interface [34]. The third semicircle in low frequency associated with Nernst diffusion process in the electrolyte was missing perhaps due to the limited frequency range employed in this study. This could also be due to a weak resistance of ion transport in electrolyte [35]. The series resistance $R_s$, which can be obtained from the lower extreme intersection point of the smaller semicircle at the horizontal axis of Nyquist plot, represents charge transfer resistance of $TiO_2$/FTO interface, the series resistance of FTO, the series resistance of platinum electrode, and resistance of external circuit. The EIS parameters which were obtained from the equivalent circuit fitting are tabulated in Table 3.

As can be seen from Table 3, $R_s$ and $R_1$ values are nearly the same in all the DSSCs. This could be due to the similar interface exists between FTO/$TiO_2$ and electrolyte/counter electrode interfaces in all three above DSSCs. Among the estimated $R_2$ values, the lowest value of 17.1 Ω was observed for the DSSC with $TiO_2$ microsphere scattering layer. This lowest value leads to an efficient electron transfer at the dye-loaded $TiO_2$ electrode/electrolyte interface which enhances photovoltaic performance of P25/MS double-layered solar cell.

The electron life time $\tau$ is obtained from the frequency value corresponds to the maximum of the Bode phase plot.

**Table 2** Photovoltaic parameters of double-layer and single-layer DSSC

| Photoanode | $J_{sc}$ (mA $cm^{-2}$) | $V_{oc}$ (mV) | *FF* (%) | $\eta$ (%) |
|---|---|---|---|---|
| P25 | 13.21 | 767.5 | 65.85 | 6.68 |
| P25/NR | 13.82 | 745.1 | 68.27 | 7.03 |
| P25/MS | 14.80 | 740.6 | 67.33 | 7.38 |

**Table 3** EIS parameters of DSSCs with double-layer and single-layer $TiO_2$photoanodes

| Photoanode | $R_s$ (Ω) | $R_1$ (Ω) | $R_2$ (Ω) | $f_{max}$ (Hz) | $\tau$ (ms) |
|---|---|---|---|---|---|
| P25 | 11.4 | 3.7 | 22.2 | 21.95 | 7.25 |
| P25/NR | 11.8 | 3.8 | 22.8 | 18.56 | 8.57 |
| P25/MS | 10.5 | 3.4 | 17.1 | 17.44 | 9.13 |

$$\tau = \frac{1}{2\pi f_{max}}$$

As can be seen from the Bode plot (Fig. 7b), the frequency corresponding to the peak value of the DSSC with P25/MS photoanode has shifted to a lower value compared with the DSSCs fabricated with other two photoanodes. By using the above corresponding frequency values the calculated life time values of the electrons ($\tau$) in above three DSSCs are also tabulated in Table 3. As can be seen from the table, the electrons in the DSSC with P25/MS structured photoanode has the longest electron life time and hence less recombination compared to the other two types of DSSCs. This is associated with better interconnected pathways for electron transfer to the electrolyte and less internal electron trap sites in the P25/MS photoanode, suggesting that efficient electron transfer which effectively enhances the $J_{sc}$ and hence the overall efficiency of the cell [36, 37].

Incident photon-to-current conversion efficiency (IPCE) measures how efficiently the solar cell converts the incident photon into current at a given wavelength. Figure 8 shows IPCE curves of P25/MS, P25/NR, and P25 DSSCs. The highest IPCE values were observed for P25/MS cell for the almost entire wavelength range. This enhancement in IPCE is essentially attributed to the increased current density of the DSSC due to efficient light absorption of the dye molecules as a result of the light scattering within the photoanode as well as due to the increased dye loading of the P25/MS photoanode.

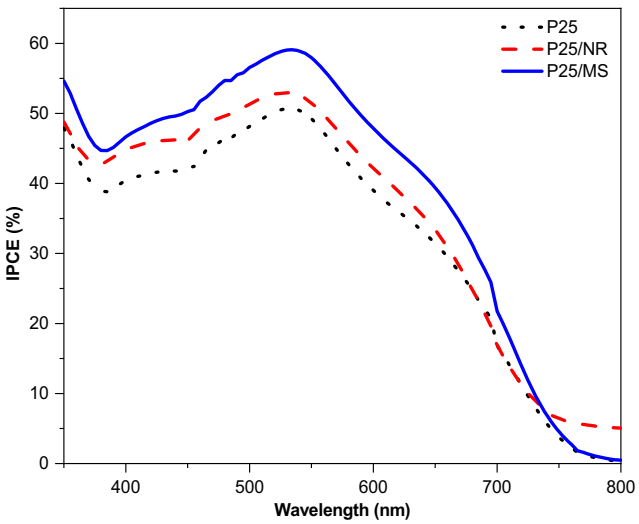


**Fig. 8** IPCE curves for P25/MS double-layer cell, P25/NR double-layer cell, and reference cell P25-based cell

## Conclusion

In summary, we have synthesized hierarchically structured $TiO_2$ submicron size spheres and $TiO_2$ nanorods and successfully employed them as scattering layers in DSSC photoanodes. It was demonstrated that the efficiency of DSSCs can be significantly enhanced by using a nanostructurally modified photoanode fabricated with hierarchically structured $TiO_2$ submicron size spheres as an efficient light scattering layer. While the DSSCs fabricated with above photoanode showed 7.38% efficiency with photo current density of 14.80 mA $cm^{-2}$, DSSCs fabricated without such a scattering layer showed 6.68% efficiency with a current density of 13.21 mA $cm^{-2}$. However, the DSSCs fabricated with $TiO_2$ nanorods as the scattering layer showed efficiency 7.03% with current density 13.82 mA $cm^{-2}$. It was also demonstrated that the enhancement in photo current density and the efficiency in DSSCs with P25/MS photoanode are evidently due to the enhanced light absorption by scattering and additional dye adsorbing by the modified photoanode with hierarchically structured $TiO_2$ submicron size spheres. In addition, it was also revealed that the decrease in the charge transfer resistance ($R_2$) of the dye-loaded $TiO_2$ P25/MS electrode/electrolyte interface and the longer electron life time in the above DSSCs further supported in this efficiency enhancement due to the lowering the electron recombination processes within the cell.

**Funding information** This project received financial support from the National Science Foundation of Sri Lanka under grant no. NSF/SCH/2019/05.

## Compliance with ethical standards

**Conflict of interest** The authors declare that they have no conflict of interest.

## References

1. O'Regan B, Grätzel M (1991) A low-cost, high-efficiency solar cell based on dye-sensitized colloidal $TiO_2$ films. Nature 353(6346): 737–740
2. Kalyanasundaram K (2010) Dye-sensitized solar cells, 1st edn. EPFL press, Lausanne
3. Yella A, Lee HW, Tsao HN, Yi C, Chandiran AK, Nazeeruddin MK (2011) Porphyrin-sensitized solar cells with cobalt (II/III)-based redox electrolyte exceed 12 percent efficiency. Science 334(6056):629–634
4. Mathew S, Yella A, Gao P, Humphry-Baker R, Curchod BFE, Ashari-Astani N et al (2014) Dye-sensitized solar cells with 13% efficiency achieved through the molecular engineering of porphyrin sensitizers. Nat Chem 6:242–247
5. Kakiage K, Aoyama Y, Yano T, Oya K, Fujisawa J, Hanaya M (2015) Highly-efficient dye-sensitized solar cells with collaborative sensitization by silyl-anchor and carboxy-anchor dyes. Chem Commu 51(88):15894–15897

6. Freitag M, Teuscher J, Saygili Y, Zhang X, Giordano F, Liska P, Hua J, Zakeeruddin SM, Moser JE, Grätzel M, Hagfeldt A (2017) Dye-sensitized solar cells for efficient power generation under ambient lighting. Nat Photonics 11(6):372–378
7. Song MY, Kim DK, Ihn KJ, Jo SM, Kim DY (2004) Electrospun $TiO_2$ electrodes for dye-sensitized solar cells. Nanotechnology 15: 1861–1865
8. Liu Z, Su X, Hou G, Bi S, Xiao Z, Jia H (2013) Mixed photoelectrode based on spherical $TiO_2$ nanorod aggregates for dye-sensitized solar cells with high short-circuit photocurrent density. RSc Adv 3:8474–8479
9. Kumari JMKW, Senadeera GKR, Dissanayake MAKL, Thotawatthage CA (2017) Dependence of photovoltaic parameters on the size of cations adsorbed by $TiO_2$ photoanode in dye-sensitized solar cells. Ionics 23(10):2895–2900
10. Ye M, Xin X, Lin C, Lin Z (2011) High efficiency dye-sensitized solar cells based on hierarchically structured nanotubes. Nano Lett 11:3214–3220
11. Senadeera GKR, Kobayashi S, Kitamura T, Wada Y, Yanagida S (2005) Versatile preparation method for mesoporous$TiO_2$ electrodes suitable for solid-state dye sensitized photocells. Bull Mater Sci Sci 28(6):635–641
12. Barbé CJ, Arendse F, Comte P, Jirousek M, Lenzmann F, Shklover V et al (1997) Nanocrystalline titanium oxide electrodes for photovoltaic applications. J Am Ceram Soc 80:3157–3171
13. Mishra A, Fischer MKR, Bäuerle P (2009) Metal-free organic dyes for dye-sensitized solar cells: from structure: property relationships to design rules. Angew Chem 48(14):2474–2499
14. Cid JJ, Yum JH, Jang SR, Nazeeruddin MK, Martínez-Ferrero E, Palomares E et al (2007) Molecular cosensitization for efficient panchromatic dye-sensitized solar cells. Angew Chem 119:8510–8514
15. Chen Y, Zeng Z, Li C, Wang W, Wang X, Zhang B (2005) Highly efficient co-sensitization of nanocrystalline $TiO_2$ electrodes with plural organic dyes. New J Chem 29(6):773–776
16. Yum J-H, Baranoff E, Kessler F, Moehl T, Ahmad S, Bessho T, Marchioro A, Ghadiri E, Moser JE, Yi C, Nazeeruddin MK, Grätzel M (2012) A cobalt complex redox shuttle for dye-sensitized solar cells with high open-circuit potentials. Nat Commun 3(1):631
17. Dissanayake MAKL, Thotawatthage CA, Senadeera GKR, Bandara TMWJ, Jayasundera WJMJSR, Mellander B-E (2012) Efficiency enhancement by mixed cation effect in dye-sensitized solar cells with PAN based gel polymer electrolyte. J Photochem Photobiol A246:29–35
18. Arof AK, Aziz MF, Noor MM, Careem MA, Bandara LRAK, Thotawatthage CA, Rupasinghe WNS, Dissanayake MAKL (2014) Efficiency enhancement by mixed cation effect in dye-sensitized solar cells with a PVdF based gel polymer electrolyte. Int J Hydrog Energy 39(6):2929–2935
19. Wang H, Sun K, Tao F, Stacchiola DJ, Hu YH (2013) 3D honeycomb-like structured graphene and its high efficiency as a counter-electrode catalyst for dye-sensitized solar cells. Angew Chem 52(35):9210–9214
20. Jo Y, Cheon JY, Yu J, Jeong HY, Han CH, Jun Y et al (2012) Highly interconnected ordered mesoporous carbon-carbon nanorod nanocomposites: Pt-free, highly efficient, and durable counter electrodes for dye-sensitized solar cells. Chem Commun 48:8057–8059
21. Murakami TN, Ito S, Wang Q, Nazeeruddin MK, Bessho T, Cesar I et al (2006) Highly efficient dye-sensitized solar cells based on carbon black counter electrodes. J Electrochem Soc 153:A2255–A2261
22. Hong W, Xu Y, Lu G, Li C, Shi G (2008) Transparent graphene/PEDOT–PSS composite films as counter electrodes of dye-sensitized solar cells. Electrochem Commun 10:1555–1558
23. Ito S, Murakami TN, Comte P, Liska P, Grätzel M, Nazeeruddin MK (2008) Fabrication of thin film dye sensitized solar cells with solar to electric power conversion efficiency over 10%. Thin Solid Films 516:4613–4619
24. Bakhshayesh AM, Mohammadi MR, Dadar H, Fray DJ (2013) Improved efficiency of dye-sensitized solar cells aided by corn-like $TiO_2$ nanowires as the light scattering layer. Electrochim Acta 90:302–308
25. Marandi M, Goudarzi Z, Moradi L (2017) Synthesis of randomly directed inclined $TiO_2$ nanorods on the nanocrystalline TiO2 layers and their optimized application in dye sensitized solar cells. J Alloys Comp 711:603–610
26. Zhu P, Nair AS, Yang S, Peng S, Ramakrishna S (2011) Which is a superior material for scattering layer in dye-sensitized solar cells - electrospun rice grain- or nanofiber-shaped $TiO_2$? J Mater Chem 21:12210–12212
27. Qiu Y, Chen W, Yang S (2010) Double-layered photoanodes from variable-size anatase $TiO_2$ nanospindles: a candidate for high-efficiency dye-sensitized solar cells. Angew Chem 49:3675–3679
28. Sauvage F, Chen D, Comte P, Huang F, Heiniger LP, Cheng YB (2010) Dye-sensitized solar cells employing a single film of mesoporous $TiO_2$ beads achieve power conversion efficiencies over 10%. ACS Nano 4:4420–4425
29. Huang F, Chen D, Zhang XL, Caruso RA, Cheng YB (2010) Dual-function scattering layer of submicrometer-sized mesoporous $TiO_2$ beads for high-efficiency dye-sensitized solar cells. Adv Funct Mater 20(8):1301–1305
30. Al-Attafi K, Nattestad A, Yamauchi Y, Dou SX, Kim JH (2017) Aggregated mesoporous nanoparticles for high surface area light scattering layer $TiO_2$ photoanodes in dye-sensitized solar cells. Sci Rep 7(1):10341
31. Kumari JMKW, Sanjeevadharshini N, Dissanayake MAKL, Senadeera GKR, Thotawatthage CA (2016) The effect of $TiO_2$ photo anode film thickness on photovoltaic properties of dye-sensitized solar cells. Ceylon J Sci 45(1):33–41
32. Akilavasan J, Al-Jassim M, Bandara J (2015) Designing nanostructured one-dimensional $TiO_2$ nanorod and $TiO_2$ nanoparticle multilayer composite film as photoanode in dye-sensitized solar cells to increase the charge collection efficiency. J Nanophoton 9(1): 093091
33. Kim YJ, Lee M, Kim H, Lim G, Choi Y, Park N-G, Kim K, Lee W (2009) Formation of highly efficient dye-sensitized solar cells by hierarchical pore generation with nanoporous $TiO_2$ spheres. Adv Mater 21:3668–3673
34. Wang Q, Moser JE, Gratzel M (2005) Electrochemical impedance spectroscopic analysis of dye-sensitized solar cells. J Phys Chem B109:14945–14953
35. Han L, Koide N, Chiba Y, Mitate T (2004) Modeling of an equivalent circuit for dye-sensitized solar cells. Appl Phys Lett 84(13): 2433–2435
36. Dissanayake MAKL, Jaseetharan T, Senadeera GKR, Thotawatthage CA (2018) A novel Pbs: Hg quantum dot sensitized highly efficient solar cells structure with triple layers $TiO_2$ photoanode. Electochim Acta 269:172–179
37. Zhang Z, Ito S, O'Regan B (2009) The electronic role of the $TiO_2$ light-scattering layer in dye-sensitized solar cells. ZeitschriftfürPhysikalischeChemie 221:319–327